



ELSEVIER

Journal of Non-Crystalline Solids 305 (2002) 247–254

JOURNAL OF
NON-CRYSTALLINE SOLIDS

www.elsevier.com/locate/jnoncrisol

Surface area, geometrical and configurational effects on permittivity of porous media

Scott B. Jones^{*}, Dani Or

Department of Plants, Soils, and Biometeorology, Utah State University, Logan, UT 84322-4820, USA

Abstract

Dielectric permittivity measurements in high surface area porous media are subject to a number of influences, including water binding effects which often lead to erroneous water content estimates. Errors are primarily due to the large disparity between the permittivity of bound (5) and free water (80). Water bound to solid surfaces exhibits a ‘thermoelectric’ effect involving temperature-dependent volume exchange between these two water phases. Particle shape and phase configuration may also reduce permittivities of porous mixtures in addition to the influence of bound water. Modeled predictions of these effects are presented and discussed and are based on a three-phase dielectric mixing model. © 2002 Elsevier Science B.V. All rights reserved.

PACS: 77.22.-d; 77.22.Gm; 51.70.+f

1. Introduction

Electromagnetic measurement of the bulk dielectric permittivity of porous media such as soils or cereal grains is used to infer water content. Measurements in high surface area materials, or in particles of high aspect ratio are influenced by bound water and dipole interactions due to particle geometry. Previous studies of thermal perturbations in wet soil samples revealed strong interactions between bound and free water, termed the ‘thermoelectric effect’ by Or and Wraith [1]. Models have been developed which combine the dielectric permittivity of bound and free water phases. Jones and Or [2] combined a surface area-

dependent bound water permittivity model with a model describing the temperature-dependent permittivity of free water to model the total water-phase permittivity. Determination of the water content of porous media (e.g., soil, cereal grains) from measured bulk permittivity, ϵ_b , is based on the dominance of the high dielectric permittivity of liquid water relative to that of solids and air. Water that is ‘bound’ to solid surfaces, is subject to surface forces that hinder its response to an imposed electromagnetic field resulting in both a lower relaxation frequency and lower ϵ_b relative to free liquid water. The first mono-layer of bound water, closest to the solid surface, is held most tightly, and has the lowest measured ϵ_b . The bulk permittivity of successive molecular water layers increases with distance from the solid surface up to that of free water at around three molecular layers [3].

^{*} Corresponding author. Tel.: +1-435 797 2175; fax: 1-435 797 2175.

E-mail address: sjones@mendel.usu.edu (S.B. Jones).

The dielectric permittivity of wet, high surface area materials (i.e., clays, starches and proteins) exhibit reduced bulk dielectric permittivities compared to materials with lower surface area at the same water content. Dielectric mixing theory offers physically based predictions of bulk permittivity based on constituent permittivities and their volumetric contributions to the mixture [4]. Particle shape may also influence electromagnetic measurements, depending on the particle aspect ratio and particle orientation (random, aligned) with respect to the applied electrical field [5] shown in Fig. 1. The shape of soil particles or any portion of cereal grains from the kernel itself, to the starch granule, to the molecular components, may influence the dielectric measurement based on each component's respective dipole moment. Starch makes up as much as 70% of the kernel of cereal grains making its water retention/binding characteristics important for modeling. Particle shape effects have been measured on individual kernels [6] and on mixtures of isotropic [7,8] and anisotropic particles [5].

The objectives of this work were to evaluate effects due to bound water, temperature, particle shape, and phase configuration on the dielectric permittivity of porous materials (e.g., wet soils and cereal grains) and to model these effects using dielectric mixing theory.

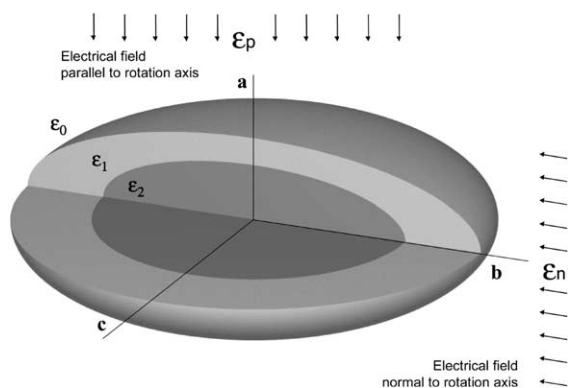


Fig. 1. Three-phase system described by a confocal oblate spheroid (core, ϵ_2 and shell, ϵ_1) contained in a background permittivity, ϵ_0 . The resulting permittivity is referenced with respect to the electrical field alignment, designated as either normal (ϵ^n) or parallel (ϵ^p) to the rotation axis, a .

2. Theoretical considerations

2.1. Temperature dependence of bound and free water

The temperature dependence of the dielectric permittivity of porous materials can be attributed largely to the effect of temperature on the water phase. The temperature-dependent permittivity of free water is described by the following expression [9]:

$$\epsilon_{fw}(T) = 78.54[1 - 4.579 \times 10^{-3}(T - 298) + 1.19 \times 10^{-5}(T - 298)^2 - 2.8 \times 10^{-8}(T - 298)^3], \quad (1)$$

where T (K) is the temperature. The temperature dependence of the bound portion of water is more complicated, especially since the boundary between bound and free water is vague. Or and Wraith [1] derived a temperature-dependent model describing bound water content (M_{bw}), expressed in terms of the bound water layer thickness, $x(T)$ (m), the specific surface area, A_s ($\text{m}^2 \text{g}^{-1}$), and the bulk density, ρ_b (g m^{-3}), of the porous medium, written as

$$M_{bw} = x(T)A_s\rho_b, \quad (2)$$

where $x(T)$ was derived from the viscosity profile of water as a function of distance from a clay surface coupled with the Debye [10] model predicting relaxation frequency of a polar liquid. Or and Wraith have used a cutoff frequency, f^* (Hz), below which bound water relaxes and thus practically does not affect a time domain reflectometer (TDR) signal. The resulting temperature-dependent bound water layer thickness, $x(T)$ (m), is computed as

$$x(T) = \frac{\alpha}{-d + T \ln \left(\frac{kT}{8\pi^2 r^3 c f^*} \right)}, \quad (3)$$

where the constants $\alpha = 1621 \text{ \AA K}$, $d = 2.047 \times 10^3 \text{ K}$, $c = 9.5 \times 10^{-7} \text{ Pa s}$, k is the Boltzmann constant ($1.38062 \times 10^{-23} \text{ J K}^{-1}$) and r (m) is the radius of the bound water molecule ($\sim 1.8\text{--}2.5 \text{ \AA}$).

2.2. Modeling the total water-phase permittivity

Separation of the water phase into bound and free water necessitates the use of a four-phase

mixing model to accommodate two water phases in addition to solid and air phases. Four-phase mixing models either do not allow for modeling of different particle shapes [11] or become too cumbersome and complicated, having numerous possible phase configurations [4]. Combining the temperature-dependent water-phase permittivity of bound and free water allows the use of a three-phase mixing model with shape effects. Functions describing the water-phase permittivity (i.e., bound and free water) were proposed by Friedman [12] and Robinson [13] based on an exponential function describing the permittivity increase with increasing water film thickness approaching the asymptotic maximum permittivity of free water. The bound water temperature-dependent expression, $x(T)$ (Eq. (3)), was coupled with Eq. (1), to describe the increase in permittivity with water layer thickness, resulting in the following expression:

$$\varepsilon_w(T) - \varepsilon_{fw}(T) \left[1 - \exp\left(\frac{-t_w}{X(T)}\right) \right], \quad (4)$$

where t_w (m) is the thickness of water on the solid surface, which can be calculated using Eq. (2) and replacing M_{bw} with M_v , the total volumetric water content, and replacing $x(T)$ with t_w (i.e., $t_w = M_v / (A_s \rho_b)$).

2.3. A three-phase dielectric mixing model

Modeling the bulk permittivity, ε , of a three-phase system consisting of inclusions comprised of a core and outer shell of confocal ellipsoids (Fig. 1) allows for accounting of particle shape effects via the depolarization factor in addition to phase configuration effects. The core, ε_2 , and the outer shell, ε_1 , are contained in a background host medium of permittivity, ε_0 . The permittivity of an isotropic three-phase confocal system of ellipsoids was derived by Sihvola and Lindell ([4], Eq. (48)) for any number of confocal ellipsoids, written as

$$\varepsilon = \varepsilon_0 + \frac{\frac{\varepsilon_0}{3} \sum_{i=p,n,n} \left(\frac{n_v \alpha^i}{\varepsilon_0} \right)}{1 - \frac{1}{3} \sum_{i=p,n,n} N_1^i \left(\frac{n_v \alpha^i}{\varepsilon_0} \right)}, \quad (5)$$

where the polarizability term in parenthesis is given as a series expansion written here for the dual, confocal ellipsoid system as

$$\frac{n_v \alpha^i}{\varepsilon_0} = (\phi_1 + \phi_2) \times \frac{\left\{ (\varepsilon_1 - \varepsilon_0) + [\varepsilon_1 + N_1^i(\varepsilon_0 - \varepsilon_1)] \frac{(\varepsilon_2 - \varepsilon_1) \frac{\phi_2}{(\phi_1 + \phi_2)}}{[\varepsilon_1 + N_2^i(\varepsilon_2 - \varepsilon_1)]} \right\}}{\left\{ [\varepsilon_0 + N_1^i(\varepsilon_1 - \varepsilon_0)] + N_1^i(1 - N_1^i)(\varepsilon_1 - \varepsilon_0) \frac{(\varepsilon_2 - \varepsilon_1) \frac{\phi_2}{(\phi_1 + \phi_2)}}{[\varepsilon_1 + N_2^i(\varepsilon_2 - \varepsilon_1)]} \right\}}, \quad (6)$$

where ϕ_1 and ϕ_2 are the volumetric fractions and N_1^i and N_2^i are the depolarization factors of the shell and core ellipsoids, respectively. Various combinations of solid, liquid and gas phases may be assigned to the core, shell and background. The depolarization factor accounts for the dipole effect arising from the particle shape-field alignment, which influences the bulk permittivity. A continuous empirical function describing the depolarization factor ranging from a disk- to a needle-shaped spheroid was fitted by Jones and Friedman [5] as

$$N^p = \frac{1}{1 + 1.6\left(\frac{a}{b}\right) + 0.4\left(\frac{a}{b}\right)^2}; \quad (7)$$

$$N^n = 0.5(1 - N^p),$$

where the depolarization factor for the electrical field aligned parallel to the axis of symmetry (rotation axis) is N^p and is N^n when normal to the axis of symmetry and where ab is the particle or kernel aspect ratio (see Fig. 1).

3. Experimental

Moist mixtures of sand and glass beads with 18% montmorillonite were uniformly packed into coaxial TDR cells [14]. After filling with the glass bead-clay mixtures, the ends were sealed using threaded PVC caps with silicone sealant. These were immersed in circulating water baths to impose multiple discrete levels of constant temperature over the range 5–50 °C. A coaxial cell filled with distilled and deionized water was included to serve as a control. Cells were maintained at a given temperature for about 3 days. Bulk dielectric

permittivity was measured using a Tektronix TDR at 0.5-h increments, and the measured replicate cell mean $\epsilon_b(T)$ were used in the model to infer specific surface area of the coaxial cell contents. The mixture specific surface areas were independently measured using EGME adsorption [15]. Accuracy of TDR-based measurements for water content are on the order of $0.02\text{--}0.03\text{ m}^3\text{ m}^{-3}$ for mineral soils.

Temperature response of corn starch permittivity was measured in a similar manner in coaxial cells by varying water content in a controlled temperature circulating water bath. Time domain reflectometry (TDR) measurements of permittivity were made using a Tektronix 1502B cable tester interfaced to a computer using WINTDR99 analysis software. In addition, independent measurements of permittivity were conducted at the same water contents using a network analyzer (HP8753C with 85070A dielectric probe) for comparison. Corn starch samples were packed into a 60 ml container which was sealed against the dielectric probe and contained in a temperature controlled cell. Samples were packed to a bulk density of 0.5 g cm^{-3} at each moisture level.

4. Results

4.1. Thermal effects of bound water

The thermodielectric effect on the bulk permittivity of water within soil was suggested by Or and Wraith [1] to be the result of an interplay between (1) the reduction in the permittivity of free water with increasing temperature, and (2) the increased permittivity brought about by the liberation of bound water to a less hindered state (i.e., greater permittivity). They modeled this effect using Eq. (3) to represent the bound water influence on the bulk dielectric constant of sand and clay mixtures illustrated in Fig. 2. They found an apparent lag in the temperature response and suggested a possible correction for this effect. Surface area was also back calculated by optimizing the thermodielectric effect on permittivity measurements.

The thermodielectric effect is further illustrated by bulk permittivity measurements in corn starch shown in Fig. 3 and in other studies [16]. Network

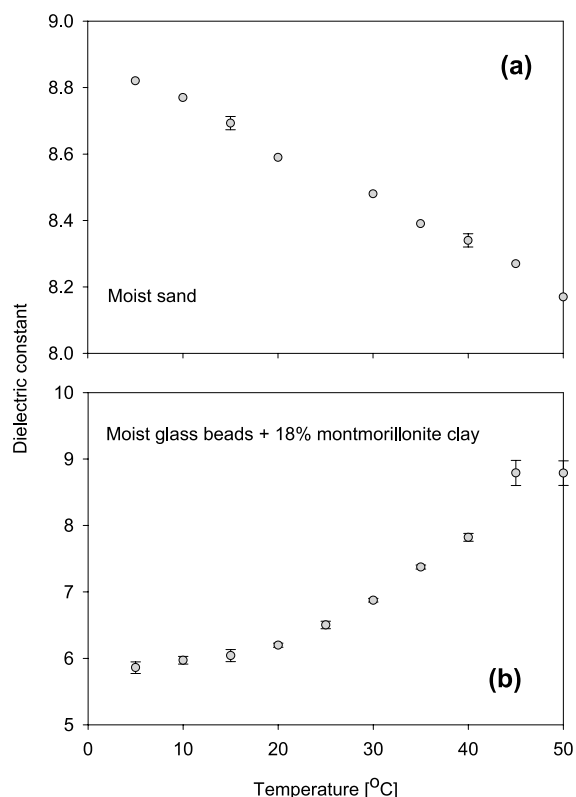


Fig. 2. Mean measured $\epsilon_b(T)$ for moist sand and glass bead–clay mixtures. Dominance of bulk water (a) for low surface area (sand at 15% mass water content), and bound water (b) for high surface area (glass beads +18% montmorillonite at 15% mass water content) are illustrated.

analyzer measurements (Fig. 3(a)) reveal a crossover in the permittivity–temperature relationship with increasing water content at about 40% (wet basis) measured at a frequency of 500 MHz. TDR measured permittivities (Fig. 3(b)) also demonstrate the effect of bound water ‘release’ throughout the measured water content range up to 50%. The reversal in the temperature–permittivity trend occurring at higher water contents occurs when starch granules approach water saturation, leading to a buildup of ‘free’ water within and eventually between granules. Near saturation, temperature increase leads to reduced permittivity of the starch, similar to the reduction in free water permittivity with increasing temperature (Eq. (1)). The large permittivity differences at mid-range moisture contents suggest an abundance of bound water

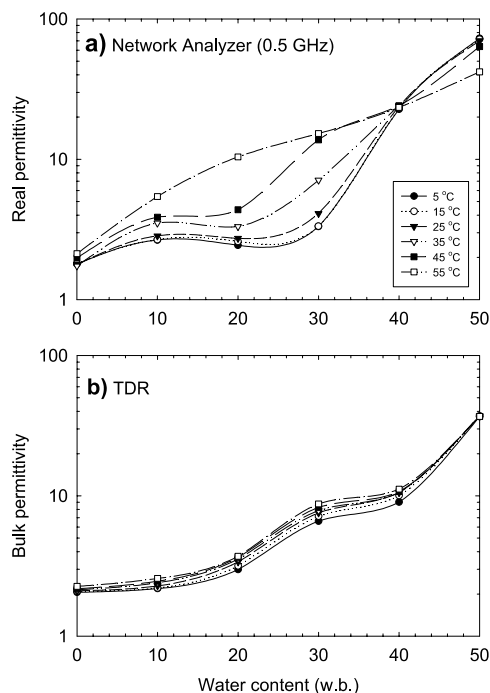


Fig. 3. Measured permittivity of corn starch as a function of water content (wet basis) using (a) a network analyzer at 0.5 GHz and (b) a TDR with temperature variations shown. Percent error relative to an average of three measurements (25 °C and 25% moisture) for the network analyzer was 7.4% and for the TDR was 3.7%.

which is liberated upon heating and the non-linear nature of the starch permittivity increase with added water also suggests an evolution of the surface area with wetting or drying. Configuration of the water associated with solids combined with surface area evolution leading to changes in bound water fraction were suggested by Jones and Or [2] to cause the distinct plateau in the permittivity-water content curve shown in Fig. 3(b) for corn starch and also noted in whole corn kernel measurements [17].

4.2. Modeling total water-phase permittivity

Measured and computed permittivities of water bound to different solid materials are shown in Fig. 4 as a function of water thickness on the solid surface. The thermoelectric effect is modeled using the water-phase permittivity relation-

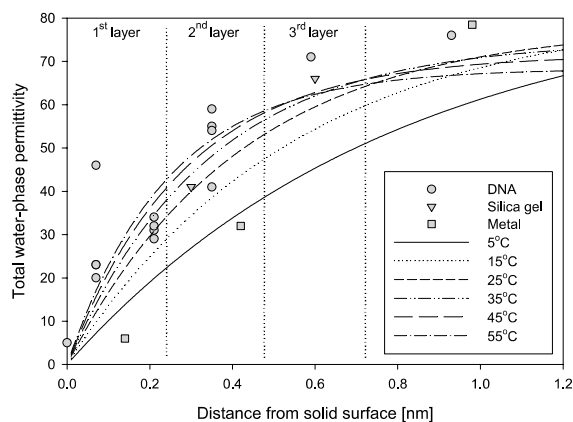


Fig. 4. Measured and modeled water-phase permittivity as a function of distance from the center of DNA [18] or distance from the surface of silica gel [19] and metal [20]. Computed temperature-dependent permittivities based on free water permittivity and on bound water radius ($r = 2.5 \times 10^{-10}$), surface area ($A_s = 400 \text{ m}^2 \text{ g}^{-1}$) and relaxation frequency ($f^* = 1 \text{ GHz}$).

ship (Eq. (4)), plotted as a function of water layer thickness (Fig. 4). For a temperature increase, this function shows both the tendency of the water-phase permittivity of the bound water fraction to increase, and also demonstrates the free water permittivity (greater than three layers) decrease with increasing temperature. Predicted permittivities for bound water are generally correlated to measured and modeled ‘bound water’ permittivities in silica gel, metal powder, and DNA.

4.3. Modeled effects on porous media bulk permittivity

4.3.1. Surface area-bound water effects

The specific surface area of a porous medium is directly related to the water binding capacity which influences the dielectric permittivity measurement. Surface areas of coarse porous media are typically orders of magnitude lower than fine textured media such as clays, proteins, or starches, whose bound water content is sufficient to produce a reduced dielectric signature. Using a solid–water–air (SWA) phase configuration, permittivities were computed using Eq. (5) where the water phase (Eq. (4)) is spread over surface areas of 0.2, 500 and 1000 $\text{m}^2 \text{ g}^{-1}$ (Fig. 5(a)). While the general trend of reduced permittivity with increasing

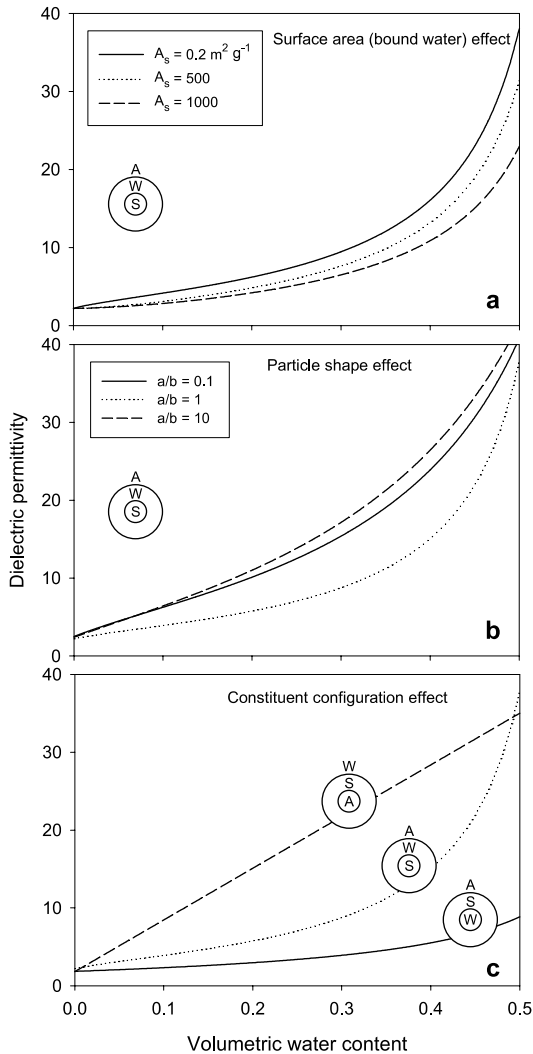


Fig. 5. Modeled permittivity using Eq. (5) with a phase configuration of SWA, demonstrating effects due to (a) surface area (A_s), (b) particle shape or aspect ratio (a/b , see Fig. 1) and (c) phase configurations comparing SWA with ASW and WSA.

surface area is produced, further work is needed to validate these predictions, which are also a function of the location of the water phase within the phase configuration where water as background has a maximum contribution on the resulting permittivity while water in the inner core plays a minimal role in the computed bulk permittivity.

Jones and Or [2] attempted to model permittivity measurements in whole kernel corn using

bound water estimates coupled with a combination of phase configurations of SWA and water–solid–air (WSA). The sigmoidal shape of the permittivity measured in corn, also noted in corn starch (Fig. (3)), suggested an evolving surface area which they attempted to model by increasing the initial surface area, A_s , with increasing water content, which required an order of magnitude increase in A_s . Predictions followed only the first few measurements, after which the permittivity was over predicted. It appeared from their results that surface area and evolution of such alone does not explain the reduction in permittivity in high surface area corn and corn starch. Other potential factors include constituent geometry and configuration.

4.3.2. Geometrical effects

Geometrical effects may be accounted for using Eq. (7), which are described as a function of particle aspect ratio. Permittivity predictions using Eq. (5) are plotted in Fig. 5(b) for three different aspect ratios of a disk ($a/b = 0.1$), a sphere ($a/b = 1$) and a needle ($a/b = 10$). Particle shape effects influencing the dielectric permittivity of cereal grains occur throughout a hierarchy of shapes and scales, from the kernel to the starch grains and their internal structure, down to the long chain and clustered polymers of amylose and amylopectin. These complex structures are also high in surface area and potentially bind a significant fraction of water. This combined effect is also a problem in clays. Jones and Friedman [5] attempted to reduce the surface area effect by measuring and modeling only particle shape effects (Fig. 6) in low surface area anisotropic packings of mica flakes. Measured permittivities in three different size fractions of mica particles (i.e., 0.25, 0.5, and 1 mm) confirmed model predictions based on particle aspect ratio (geometry) and electrical field alignment as determined by probe orientation. Using Eq. (5) and a combination of phase configurations they modeled the wet mica permittivity using an average aspect ratio of 1/25 and two different porosities of 0.7–0.8 to capture the porosity range of mica. At mid-range water contents, measured data of ϵ^p is approximately half of the ϵ^n measurements. Reduced permittivity measure-

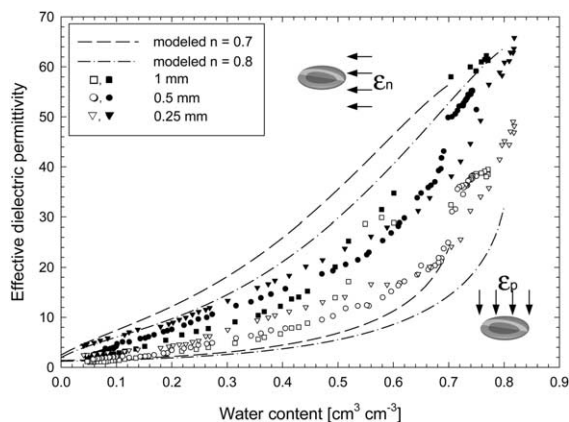


Fig. 6. Measured geometrical effect on bulk permittivity of layered mica flakes [5] (diameters of 0.25, 0.5, and 1 mm) for electrical field alignment normal (ϵ^n = empty symbols) and parallel (ϵ^p = filled symbols) to the mica's rotation axis (see Fig. 1). Modeled predictions based on Eq. (5) are depicted by lines using porosities (n) of 0.7 and 0.8.

ments in high surface area materials (e.g., clays) have been typically attributed to bound water effects. The reduction in permittivity in mica which have a very low specific surface area ($A_s < 0.06 \text{ m}^2 \text{ g}^{-1}$), can be attributed primarily to geometrical effects arising from the depolarizing influence of these high aspect ratio ($a/b = 1/25$) particles.

4.3.3. Phase configuration effects

The influence of phase configuration within a given mixing model will be dependent upon the assumptions used in deriving the formula. For the three-phase mixing model described here (Eq. (5)), phase configuration has a substantial impact on permittivity prediction as demonstrated in Fig. 5(c). As the water phase moves from outside to inside, the resulting bulk permittivity is reduced significantly owing to the large dielectric of water compared to those of solids and air. The configuration of water, solids and air within a porous medium is of a complex and highly variable nature and a likely scenario is that a combination of phase configurations exists. Averaging the computed permittivities from a set of phase configurations has been employed in soils and cereal grains. This approach was used successfully to model the three-

phase system of moist soil combining configurations of air–solid–water (ASW) and SWA using an effective medium approximation coupled with bound water predictions [12]. Adding particle shape effects to Friedman's approach, Jones and Friedman [5] found an over-prediction of particle shape effects on permittivity measurements citing particle-field misalignment and configurational effects as possible causes (Fig. 6). Jones and Or [2] combined SWA and WSA configurations to describe the permittivity of cereal grains. After applying a sigmoidal weighting function to the fractional content of SWA and WSA configurations, they found an improved fit to permittivity measurements of field corn. The justification for their approach was linked to kernel swelling or shrinking that occurs throughout the hierarchy of geometries contained in the starch grain, which comprises about 70% of the kernel. Kernel constituents may expand, unfold and relax during kernel desiccation which is accompanied by a change in kernel shape and volume. Leopold [21] demonstrated volume increases in soybean with hydration which were substantially greater than the weight of water imbibed suggesting that polymeric seed constituents unfold with hydration which they suggested is a mechanism for increased surface area or evolving water-phase configuration. Further efforts to identify and separate these competing and perhaps confounding effects of bound water, particle shape and water-phase configuration is recommended for future research.

5. Conclusions

Several effects which influence dielectric permittivity measurements have been identified through measurements and as suggested in the analysis of results. The thermodielectric effect was observed in high surface area media of clays and corn starch (major constituent of cereal grains). This mechanism has been identified as a source for determining surface area and bound water content. Particle shape effects which have been measured in low-surface area media are a function of particle geometry and electrical field alignment. Bound water and geometrical effects, including phase

configuration, may be incorporated into three-phase dielectric mixing models for predicting the bulk permittivity of wet porous media. Any one of these effects and combinations thereof appear to contribute to reduced dielectric signatures in porous media, which without properly accounting for will lead to errors in water content estimation.

Acknowledgements

Partial funding was provided by the Israel–US Binational Agricultural Research and Development (BARD) Fund (Project IS-2839-97). We gratefully acknowledge research grants from Campbell Scientific and HarvestMaster (Logan, UT) and Pioneer Hi-Bred International (Johnston, IA).

References

- [1] D. Or, J.M. Wraith, *Water Resour. Res.* 35 (1999) 371.
- [2] S.B. Jones, D. Or, in: *Proceedings of the fourth International Conference Electromagnetic Wave Interaction with Water and Moist Substances*, Weimar, Germany, May 13–16, 2001, p. 46.
- [3] J.O. Bockris, E. Giladi, K. Muller, *J. Chem. Phys.* 44 (1966) 1445.
- [4] A. Sihvola, I.V. Lindell, *J. Electromagnetic Waves Appl.* 4 (1990) 1.
- [5] S.B. Jones, S.P. Friedman, *Water Resour. Res.* 36 (2000) 2821.
- [6] A.W. Kraszewski, S.O. Nelson, in: A.W. Kraszewski (Ed.), *Microwave Aquametry*, IEEE, NY, 1996, p. 177.
- [7] R.W. Sillers, *J. Inst. Elect. Eng.* 80 (1936) 378.
- [8] J.M. Kelley, J.O. Stenoien, D.E. Isbell, *J. Appl. Phys.* 24 (1953) 258.
- [9] R.C. Weast, *CRC Handbook of Chemistry and Physics*, CRC Press, Boca Raton, FL, 1986.
- [10] P. Debye, *Polar Molecules*, Dover, Mineola, NY, 1929.
- [11] M.C. Dobson, F.T. Ulaby, M.T. Hallikainen, M.A. El-Rayes, *IEEE Trans. Geosci. Remote Sens.* GE-23 (1985) 35.
- [12] S.P. Friedman, *Water Resour. Res.* 34 (1998) 2949.
- [13] D.A. Robinson, *J. Hydrol.* 255 (1–4) (2002) 39.
- [14] J.M. Wraith, D. Or, in: *Proceedings of the Third Workshop on Electromagnetic Wave Interaction with Water and Moist Substances*, April 12–13, 1999, Athens, GA, 1999, p. 222.
- [15] D.L. Carter, M.M. Mortland, W.E. Kemper, *Specific surface*, in: A. Klute (Ed.), *Methods of Soil Analysis, Part 1, Physical and Mineralogical Methods*, 2nd Ed., ASA, Madison, WI, 1986, p. 413.
- [16] M.K. Ndife, G. Sumnu, L. Bayindirli, *Food Res. Int.* 31 (1998) 43.
- [17] R.N. Jones, H.E. Bussey, W.E. Little, R.F. Mezker, *National Bureau of Standards Report*, NBSIR 78-897, Boulder, CO, 1978.
- [18] G. Lamm, G.R. Pack, *Int. J. Quant. Chem.* 65 (1997) 1087.
- [19] J.M. Thorp, *Trans. Faraday Soc.* 55 (1959) 442.
- [20] J.O.M. Bockris, M.A.V. Devanathan, K. Muller, *Proc. R. Soc. (London)* A274 (1963) 55.
- [21] A.C. Leopold, *Plant Physiol.* 73 (1983) 677.